CYBERNETICS AND PHYSICS, VOL. 1, NO. 3, 2012 , 216–222

MASTER-SLAVE AND MUTUAL MULTIPLE SYNCHRONIZATION FOR MULTI-ROTOR VIBRATION UNITS

Olga Tomchina, Viktoria Galitskaya, Dmitry Gorlatov, Jamal Bagaev
Machine-Building Institute
Saint Petersburg, Russia

Abstract

Two algorithms for multiple synchronization of multi-rotor vibration units are proposed. The performance of the proposed systems is analyzed by computer simulation for model of the 3-rotor vibration set-up. The main contribution of the paper is design and numerical analysis of control algorithms providing stable multiple synchronous mode in multi-rotor vibration units with different multiplicities.

Key words

Multiple synchronization, multi-rotor vibration unit, control algorithm.

1 Introduction

A conventional way to increase performance of vibration units for screening and vibrotransportation with several vibroactuators is to improve the quality of the hardware e. g. increasing the number of the vibroactuators. One of the main arising problems is keeping stable synchronous operation mode in order to achieve maximum amplitude of the platform vibrations under changing operation conditions and maximum vibrotransportation velocity. An usual way of solving that problem is based on exploiting self-synchronization phenomenon discovered by I. I. Blekhman [Blekhman, 2000], [Blekhman, 2012] who proposed a unified view on synchronization. Significant results on stability study of synchronous mode for mechanical systems were obtained in [Gauthier and Micheau, 2008], [Pogromsky, Belykh and Nijmeijer, 2003], [Wu, Wang and Li, 2012], [Ulrichs, Mann and Parlitz, 2009], [Pena-Ramirez, Fey and Nijmeijer, 2012], [Wang, Zhao and Yao, 2012], [Czolczynski, Perlikowski and Stefanski, 2012]. The results of the above mentioned works require however that the plant model is known rather accurately.

However in some cases synchronization is not stable enough. It happens e. g. if one needs to provide the desired phase shifts or when multiple synchronization is needed. In such cases the controlled synchronization may help.

A systematic approach to controlled synchronization of vibration units based on speed-gradient control algorithms was proposed in [Andrievsky, Blekhman, Bortsov, *et al.*, 2001], [Blekhman, Fradkov, Tomchina and Bogdanov, 2002], [Tomchina and Kudryavtseva, 2005], [Fradkov, Andrievsky and Boykov, 2012]. Controlled synchronization provides additional opportunities, especially for vibrotransportation of materials. It may keep constant the ratio of average velocities and/or phases of vibroactuators.

Multiple synchronous mode introduces an asymmetry into the system and gains efficiency of vibrotransportation, since it allows to avoid congestion at the system output. It is especially important for subtle technologies like transportation of powdered, wet and adhesive materials. In addition, presence of multiple rotation frequencies in the system allows technology equipment to perform transportation (with low frequency vibrations) and screening/separation of dry materials simultaneously. Unlike the simple synchronization modes which can arise spontaneously and remain as the parameters change in a small area, the multiple synchronization mode is sensitive to vibration unit parameter variations. Therefore a stable multiple synchronous mode can only be achieved by means of advanced control.

In this paper two algorithms for multiple synchronization of multi-rotor vibration unit are proposed. The design is based on the speed-gradient method [Fradkov, 2007] applied previously to control of different mechanical systems including vibration units [Andrievsky, Blekhman, Bortsov, *et al.*, 2001], [Blekhman, Fradkov, Tomchina and Bogdanov, 2002]. The performance of the proposed system is analyzed by computer simulation for model of the 3-rotor vibration set-up.

2 Control Algorithm for Multiple Synchronization

First of all let us introduce the idea of Speed-Fradient (SG) algorithm, following [Andrievsky, Blekhman, Bortsov, *et al* 2001], [Fradkov, 2007]. Let the controlled system dynamics be described by the state space differential equations

$$dz/dt = F(z,M),$$

where z is n-dimensional state vector (e. g. for mechanical systems described by Lagrange 2-nd kind equations z consists of generalized coordinates and their derivatives); M is the vector of controlling variables (torques). Let the control goal be described by the non-negative goal function (GF) $Q(z) > 0$:

$$Q(z(t)) \to 0 \ as \ t \to \infty.$$

Then the SG control algorithm is as follows:

$$M = -\gamma \nabla_M \dot{Q}(z),$$

where notation $\dot{Q}(z) = \frac{dQ(z)}{dt}$ stands for the time derivative of GF along trajectories of the controlled system, ∇ is a symbol of gradient (vector of partial derivatives), $\gamma > 0$ is a positive gain.

According to [Blekhman, Fradkov, Tomchina and Bogdanov, 2002], [Fradkov, 2007] multiple synchronization means achievement of either the relation $\dot{\varphi}_s/n_s - \dot{\varphi}_r/n_r = 0$ (multiple frequency synchronization) or $\frac{\varphi_s}{n_s} - \frac{\varphi_r}{n_r} = L_{sr}$; $s,\ r = 1,\ldots,k$ for some constant L_{sr} (multiple phase synchronization) or both, where n_s, n_r are given multiplicities for frequencies.

To apply SG method one needs to choose the goal function, evaluate its speed of its change along trajectories of controlled system and to change control in the direction of the gradient of the evaluated speed. The first suggestion is to choose the goal function as follows:

$$Q(z) = \left\{0.5(1-\alpha)(H-H^*)^2 + \sum_{s,r\neq s}^{k} \alpha_{s,r}\,(\dot{\varphi}_s/n_s \pm \dot{\varphi}_r/n_r)^2\right\}, \quad (1)$$

where z is the state vector of the system; $\dot{\varphi}_i$ are angular velocities of unbalanced rotors (vibroactuators), $\alpha_{s,r} > 0$, $\sum_{s,r>s}^{k} \alpha_{s,r} = \alpha$, $0 < \alpha < 1$ are weighting coefficients; H is the total mechanical energy, H^* is the desired level of H. Obviously if the goal is achieved then $Q(z) = 0$, otherwise $Q(z) > 0$. If $Q(z) = 0$ then $= {}^*$, it provides required rotor velocities and multiple synchronization relation $\dot{\varphi}_s/n_s = \pm\dot{\varphi}_r/n_r$. Note that at the first stage of design we have neglected the friction. Applying the SG method the speed of changing (1) along trajectories of controlled system and the gradient of the speed with respect to controlling variables (torques) are evaluated. Then the designed control algorithm is as follows:

$$M_s = \gamma_s\{(1-\alpha)(H-H^*)\,\dot{\varphi}_s \pm \pm\sum_r \alpha_{sr}\,(\dot{\varphi}_s/n_s \pm \dot{\varphi}_r/n_r)\}, \quad (2)$$

where M_s are controlling torques, $\gamma_s > 0$ are control gains, $s = 1,\ldots,k$. The control algorithm (2) is called the *mutual synchronization algorithm*.

A different approach is based on the goal function

$$Q(z) = 0.5\{(1-\alpha)(H-H^*)^2 + + \sum_{r>1}^{k} \alpha_{1,r}\,(\dot{\varphi}_1/n_1 \pm \dot{\varphi}_r/n_r)^2\}. \quad (3)$$

Applying the SG method, we arrive at the following control algorithm:

$$M_s = -\gamma_s\{(1-\alpha)(H-H^*)\,\dot{\varphi}_s \pm \pm\sum_r \alpha_{1,r}\,(\dot{\varphi}_1/n_s \pm \dot{\varphi}_r/n_r)\}. \quad (4)$$

Here the rotors indexed with the numbers $r = 2,\ldots,k$ are pushed to synchronize with the first rotor. The control algorithm (4) is called the *synchronization algorithm with the leading rotor*.

Efficiency of the proposed algorithms was analyzed for 3-rotor vibration unit [Andrievsky, Blekhman, Bortsov, *et al.* 2001] model with 6 degrees of freedom taking into account 3 degrees of freedom for supporting body (Fig. 1).

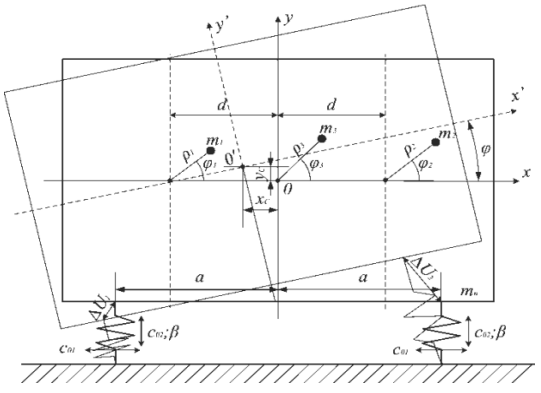

Figure 1. The kinematic scheme of controlled mechanical system.

Here $\varphi_1, \varphi_2, \varphi_3$ are rotation angles of the rotors measured from the horizontal position, x_c, y_c are the horizontal and vertical displacement of the supporting body

from the equilibrium position, $m_i = m$, are the masses of the rotors, J_1, J_2, J_3 are the inertia moments of the rotors, $\rho_i = \rho$ is the eccentricity of rotors, c_{01}, c_{02} are the horizontal and vertical spring stiffness, g is the gravitational acceleration, m_0 is the total mass of the unit, β is the damping coefficient, k_c the friction coefficient in the bearings, M_1, M_2, M_3 are the motor torques (controlling variables). We will assume that rotor shafts are orthogonal to the motion of the support.

The unit dynamics can be described by the Lagrange second kind equations

$$\begin{gathered}
m_0\ddot{x}_c - \ddot{\varphi}m\rho\,(\sin(\varphi+\varphi_1)+\sin(\varphi+\varphi_2)+\\
\sin(\varphi+\varphi_3)) - \ddot{\varphi}_1 m\rho\sin(\varphi+\varphi_1) -\\
\ddot{\varphi}_2 m\rho\sin(\varphi+\varphi_2) - \ddot{\varphi}_3 m\rho\sin(\varphi+\\
\varphi_3) - \dot{\varphi}^2 m\rho\,(\cos(\varphi+\varphi_1)+\cos(\varphi+\varphi_2)+\\
+\cos(\varphi+\varphi_3)) - \dot{\varphi}_1^2 m\rho\cos(\varphi+\varphi_1) -\\
\dot{\varphi}_2^2 m\rho\cos(\varphi+\varphi_2) - \dot{\varphi}_3^2 m\rho\cos(\varphi+\varphi_3) -\\
2\dot{\varphi}\dot{\varphi}_1 m\rho\cos(\varphi+\varphi_1) - 2\dot{\varphi}\dot{\varphi}_2 m\rho\cos(\varphi+\varphi_2) -\\
2\dot{\varphi}\dot{\varphi}_3 m\rho\cos(\varphi+\varphi_3) + 2c_{01}x_c + \beta\dot{x}_c = 0;
\end{gathered}$$

$$\begin{gathered}
m_0\ddot{y}_c + \ddot{\varphi}m\rho(\cos(\varphi+\varphi_1)+\cos(\varphi+\varphi_2)+\\
\cos(\varphi+\varphi_3)) - \ddot{\varphi}_1 m\rho\cos(\varphi+\varphi_1) -\\
\ddot{\varphi}_2 m\rho\cos(\varphi+\varphi_2) - \ddot{\varphi}_3 m\rho\cos(\varphi+\varphi_3) -\\
\dot{\varphi}^2 m\rho(\sin(\varphi+\varphi_1)+\sin(\varphi+\varphi_2)+\sin(\varphi+\varphi_3)) -\\
\dot{\varphi}_1^2 m\rho\sin(\varphi+\varphi_1) - \dot{\varphi}_2^2 m\rho c\sin(\varphi+\varphi_2) -\\
\dot{\varphi}_3^2 m\rho\sin(\varphi+\varphi_3) - 2\dot{\varphi}\dot{\varphi}_1 m\rho\sin(\varphi+\varphi_1) -\\
2\dot{\varphi}\dot{\varphi}_2 m\rho\sin(\varphi+\varphi_2) - 2\dot{\varphi}\dot{\varphi}_3 m\rho\sin(\varphi+\varphi_3) +\\
m_0 g + 2c_{02}y_c + \beta\dot{y}_c = 0;
\end{gathered}$$

$$\begin{gathered}
-\ddot{x}_c m\rho\,(\sin(\varphi+\varphi_1)+\sin(\varphi+\varphi_2)+\sin(\varphi+\varphi_3)) +\\
\ddot{y}_c m\rho\,(\cos(\varphi+\varphi_1)+\cos(\varphi+\varphi_2)+\cos(\varphi+\varphi_3)) +\\
\ddot{\varphi}\,(J+J_1+J_2+J_3-2dm\rho\,(\cos\varphi_1-\cos\varphi_2)) +\\
\ddot{\varphi}_1(J_1 - dm\rho\cos\varphi_1) + \ddot{\varphi}_2(J_2+dm\rho\cos\varphi_2) + \ddot{\varphi}_3 J_3 +\\
\dot{\varphi}_1^2 dm\rho\sin\varphi_1 - \dot{\varphi}_2^2 dm\rho\sin\varphi_2 + 2dm\rho\dot{\varphi}\dot{\varphi}_1\sin\varphi_1 -\\
2dm\rho\dot{\varphi}\dot{\varphi}_2\sin\varphi_2 + m\rho g(\cos(\varphi+\varphi_1)+\cos(\varphi+\varphi_2)+\\
+\cos(\varphi+\varphi_3)) + c_{03}\varphi + \beta\dot{\varphi} = 0;
\end{gathered} \tag{5}$$

$$\begin{gathered}
-\ddot{x}_c m\rho\sin(\varphi+\varphi_1) + \ddot{y}_c m\rho\cos(\varphi+\varphi_1) +\\
\ddot{\varphi}(J_1 - dm\rho\cos\varphi_1) + \ddot{\varphi}_1 J_1 - \dot{\varphi}^2 dm\rho\sin\varphi_1 +\\
m\rho g\cos(\varphi+\varphi_1) + k_c\dot{\varphi}_1 = M_1;
\end{gathered}$$

$$\begin{gathered}
-\ddot{x}_c m\rho\sin(\varphi+\varphi_2) + \ddot{y}_c m\rho\cos(\varphi+\varphi_2) +\\
\ddot{\varphi}(J_2 + dm\rho\cos\varphi_1) + \ddot{\varphi}_2 J_2 + \dot{\varphi}^2 dm\rho\sin\varphi_2 +\\
m\rho g\cos(\varphi+\varphi_2) + k_c\dot{\varphi}_2 = M_2;
\end{gathered}$$

$$\begin{gathered}
-\ddot{x}_c m\rho\sin(\varphi+\varphi_3) + \ddot{y}_c m\rho\cos(\varphi+\varphi_3) +\\
\ddot{\varphi}J_3 + \ddot{\varphi}_3 J_3 + m\rho g\cos(\varphi+\varphi_3) + k_c\dot{\varphi}_3 = M_3.
\end{gathered}$$

Kinetic and potential energies T and Π are as follows:

$$\begin{gathered}
T = 0.5m_0(\dot{x}_c^2+\dot{y}_c^2) + 0.5\dot{\varphi}^2\,(J+J_1+J_2+J_3 -\\
2dm\rho\,(\cos\varphi_1-\cos\varphi_2)) + 0.5J_1\dot{\varphi}_1^2 + 0.5J_2\dot{\varphi}_2^2 +\\
0.5J_3\dot{\varphi}_3^2 + \dot{\varphi}\dot{\varphi}_1(J_1 - dm\rho\cos\varphi_1) +\\
\dot{\varphi}\dot{\varphi}_2(J_2+dm\rho\cos\varphi_2) + \dot{\varphi}\dot{\varphi}_3 J_3 -\\
\dot{x}_c\dot{\varphi}m\rho(\sin(\varphi+\varphi_1)+\sin(\varphi+\varphi_2)+\sin(\varphi+\varphi_3)) +\\
\dot{y}_c\dot{\varphi}m\rho(\cos(\varphi+\varphi_1)+\cos(\varphi+\varphi_2)+\cos(\varphi+\varphi_3)) -\\
\dot{x}_c\dot{\varphi}_1 m\rho\sin(\varphi+\varphi_1) + \dot{y}_c\dot{\varphi}_1 m\rho\cos(\varphi+\varphi_1) -\\
\dot{x}_c\dot{\varphi}_2 m\rho\sin(\varphi+\varphi_2) + \dot{y}_c\dot{\varphi}_2 m\rho\cos(\varphi+\varphi_2) -\\
\dot{x}_c\dot{\varphi}_3 m\rho\sin(\varphi+\varphi_3) + \dot{y}_c\dot{\varphi}_3 m\rho\cos(\varphi+\varphi_3),
\end{gathered}$$

$$\begin{gathered}
\Pi = m_0 g y_c + m\rho g(\sin(\varphi+\varphi_1)+\sin(\varphi+\varphi_2)+\\
\sin(\varphi+\varphi_3)) + c_{01}(x_c^2 + a^2\cos^2\varphi)^2 +\\
c_{02}(y_c^2 + a^2\sin^2\varphi)^2,
\end{gathered}$$

$$H = T + \Pi.$$

Simulation results for 3-rotor vibration unit (5) with conventional control ($M_i = const$) are presented in Fig. 2–Fig. 6. In Fig. 2 the plots for double self-synchronization mode for 3-rotor vibration unit with $M_1 = M_2 = 2N\cdot m, M_3 = 4N\cdot m$.

It is seen from the plots of the multiple velocity differences and the multiple phase shift (Fig. 2, Fig. 3) that the multiple self-synchronization is established:

$$\varphi_i/n_i - \varphi_j/n_j \to const; \Delta\dot{\varphi} = (\dot{\varphi}_i/n_i - \dot{\varphi}_j/n_j) \to 0.$$

Designation of rotor speeds on figures $\omega_i = \dot{\varphi}_i$.

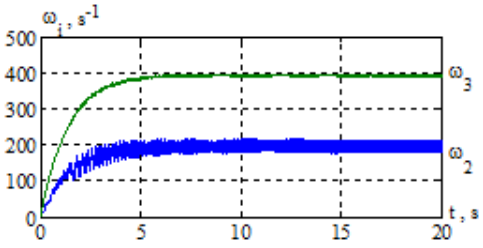

Figure 2. Plots of velocity for 2-nd and 3-rd rotors.

However even small change of relative rotor positions on the supporting body ($d = var$) may suppress self-synchronization (Fig. 4). It is seen from the plot of the multiple velocity differences that $(\dot{\varphi}_i/n_i - \dot{\varphi}_j/n_j) \neq 0$.

Moreover, the closer given speeds of rotors are to a resonant frequency (identified as a vibration frequency of a carrier body), the more unstable multiple synchronization mode appears to be due to capture of the speed at a subresonant frequency (Sommerfeld's effect). Even simple synchronization mode

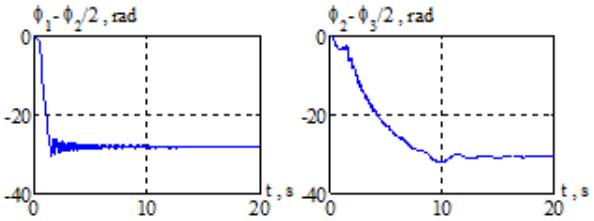

Figure 3. Plots of the multiple phase shifts ($d = 0.1m$; $J = 0.8\,kgm^2$).

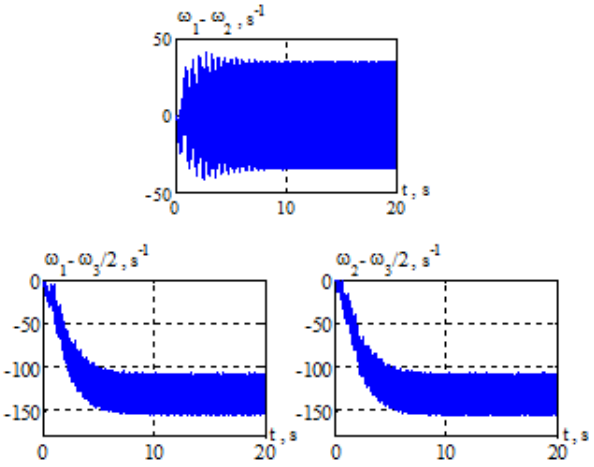

Figure 4. Plots of the multiple velocity difference ($d = 0.2m$).

($n_i = 1$, $i = 1,2,3$), at which all of three rotors are given equal-in-magnitude torques, does not take place at all cases. Fig.5 and Fig.6 show angular velocity ($\dot{\varphi}_1$, $\dot{\varphi}_2$, $\dot{\varphi}_3$) diagrams with torque values of $M_i = 2.7N \cdot m$ and $M_i = 3N \cdot m$, accordingly.

Simulation results for $d = 0.2$ m, are presented in Fig. 4.

As seen in diagrams, if values of controlling torques are $M_i = 3N \cdot m$, then the first rotor ($\dot{\varphi}_1$) in Fig. 5 does not move inside above resonance area $\omega >> \omega_{res}$, where $\omega_{res} = 30s^{-1}$, i. e. speed of rotor is captured. This effect is called the Sommerfeld's effect. Two other rotors move inside the above–resonance area, thus rotor speeds remain different, i. e. synchronization is absent. At the higher torque values all of three rotors are rotating at the same speed and all of them fall into the above–resonance mode (Fig. 6). Though speed values of rotors with minimum torque, which allows moving over resonance, equal to $\dot{\varphi}_i = 300s^{-1}$, and speed range from $\omega_{res} = 30s^{-1}$ to $300s^{-1}$ is out of achievable work speed region. The two-rotor vibration unit has similar region of "nacheivable" above–resonance speeds.

To ensure the stable multiple synchronization of three rotors in a 3-rotor vibrational unit two control algorithms are specified from (2), (4). The first algorithm is based upon the functional (1) where all pairs of velocity differences are taken into account. The algorithm

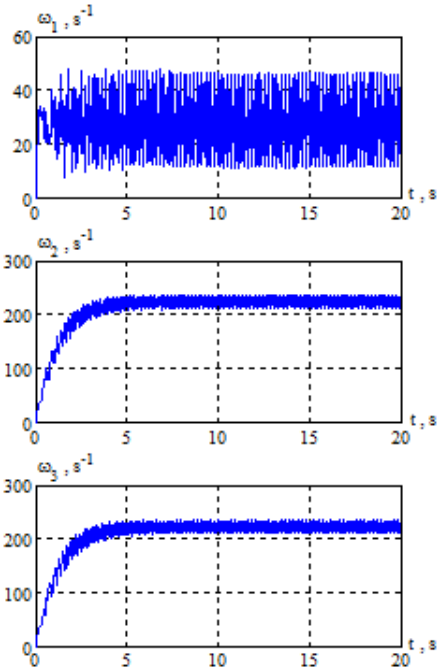

Figure 5. The results of three-rotor model analysis with $M_i = 2.7N \cdot m$.

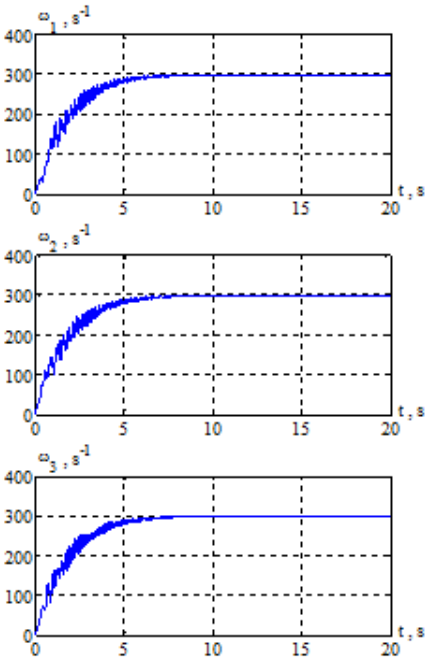

Figure 6. The results of three-rotor model analysis with $M_i = 3N \cdot m$.

looks as follows:

$$Q(z) = 0.5\left\{(1-\alpha)(H-H^*)^2 + \alpha_{12}\left(\frac{\dot{\varphi}_1}{n_1} \pm \frac{\dot{\varphi}_2}{n_2}\right)^2 + \alpha_{13}\left(\frac{\dot{\varphi}_1}{n_1} \pm \frac{\dot{\varphi}_3}{n_3}\right)^2 + \alpha_{23}\left(\frac{\dot{\varphi}_2}{n_2} \pm \frac{\dot{\varphi}_3}{n_3}\right)^2\right\}. \quad (6)$$

$$\begin{cases} \tilde{M}_1 = -\gamma_1 \left\{ (1-\alpha)\left(\tilde{H}-H^*\right)\dot{\varphi}_1 + \frac{\alpha_{12}}{J_1 n_1}\left(\frac{\dot{\varphi}_1}{n_1} \pm \frac{\dot{\varphi}_2}{n_2}\right) + \right. \\ \qquad \left. \frac{\alpha_{13}}{J_1 n_1}\left(\frac{\dot{\varphi}_1}{n_1} \pm \frac{\dot{\varphi}_3}{n_3}\right) \right\}; \\ \tilde{M}_2 = -\gamma_2 \left\{ (1-\alpha)\left(\tilde{H}-H^*\right)\dot{\varphi}_2 \pm \frac{\alpha_{12}}{J_2 n_2}\left(\frac{\dot{\varphi}_1}{n_1} \pm \frac{\dot{\varphi}_2}{n_2}\right) + \right. \\ \qquad \left. \frac{\alpha_{23}}{J_2 n_2}\left(\frac{\dot{\varphi}_2}{n_2} \pm \frac{\dot{\varphi}_3}{n_3}\right) \right\}; \\ \tilde{M}_3 = -\gamma_3 \left\{ (1-\alpha)\left(\tilde{H}-H^*\right)\dot{\varphi}_3 \pm \frac{\alpha_{13}}{J_3 n_3}\left(\frac{\dot{\varphi}_1}{n_1} \pm \frac{\dot{\varphi}_3}{n_3}\right) \pm \right. \\ \qquad \left. \frac{\alpha_{23}}{J_3 n_3}\left(\frac{\dot{\varphi}_2}{n_2} \pm \frac{\dot{\varphi}_3}{n_3}\right) \right\}. \end{cases} \tag{7}$$

The second control algorithm based upon the functional (3) is as follows:

$$Q(z) = 0.5\left\{ (1-\alpha)\left(H-H^*\right)^2 + \alpha_{12}\left(\frac{\dot{\varphi}_1}{n_1} \pm \frac{\dot{\varphi}_2}{n_2}\right)^2 + \right. \\ \left. \alpha_{13}\left(\frac{\dot{\varphi}_1}{n_1} \pm \frac{\dot{\varphi}_3}{n_3}\right)^2 \right\}. \tag{8}$$

$$\begin{cases} \tilde{M}_1 = -\gamma_1 \left\{ (1-\alpha)\left(\tilde{H}-H^*\right)\dot{\varphi}_1 + \frac{\alpha_{12}}{J_1 n_1}\left(\frac{\dot{\varphi}_1}{n_1} \pm \frac{\dot{\varphi}_2}{n_2}\right) + \right. \\ \qquad \left. \frac{\alpha_{13}}{J_1 n_1}\left(\frac{\dot{\varphi}_1}{n_1} \pm \frac{\dot{\varphi}_3}{n_3}\right) \right\}; \\ \tilde{M}_2 = -\gamma_2 \left\{ (1-\alpha)\left(\tilde{H}-H^*\right)\dot{\varphi}_2 \pm \frac{\alpha_{12}}{J_2 n_2}\left(\frac{\dot{\varphi}_1}{n_1} \pm \frac{\dot{\varphi}_2}{n_2}\right) \right\}; \\ \tilde{M}_3 = -\gamma_3 \left\{ (1-\alpha)\left(\tilde{H}-H^*\right)\dot{\varphi}_3 \pm \frac{\alpha_{13}}{J_3 n_3}\left(\frac{\dot{\varphi}_1}{n_1} \pm \frac{\dot{\varphi}_3}{n_3}\right) \right\}. \end{cases} \tag{9}$$

Obviously, in terms of implementation, algorithm (9) is simpler. However algorithm (7) also has some benefits. For example, as seen from simulation results for simple synchronization ($n_i = 1,\ i = 1,2,3$), algorithm (7) allows us to narrow the after-resonance zone of speeds unreachable for running at synchronous mode (Fig. 7).

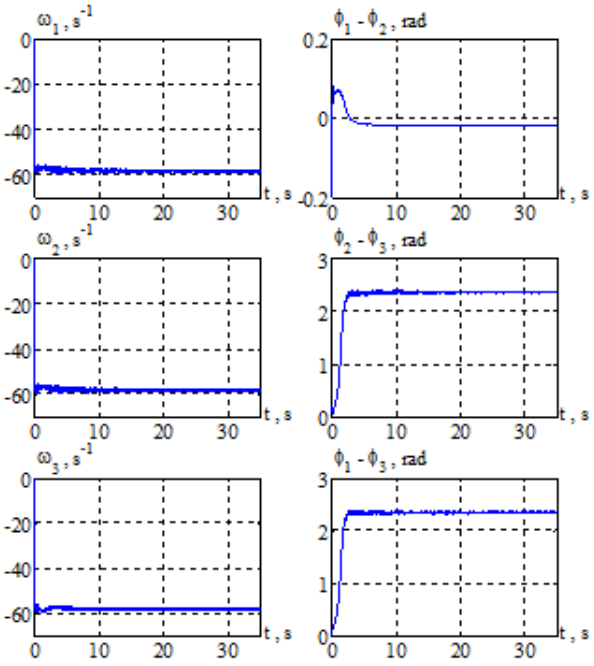

Figure 7. Three-rotor model simulation results for algorithm (7) with $n_i = 1,\ i = 1,2,3$.

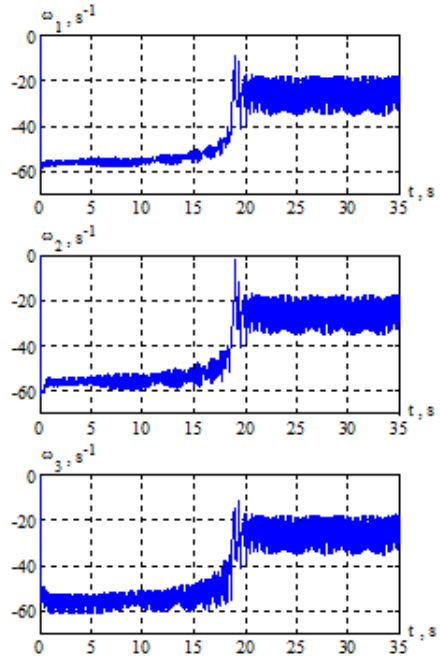

Figure 8. Three-rotor model simulation results using an algorithm (9) with $n_i = 1,\ i = 1,2,3$.

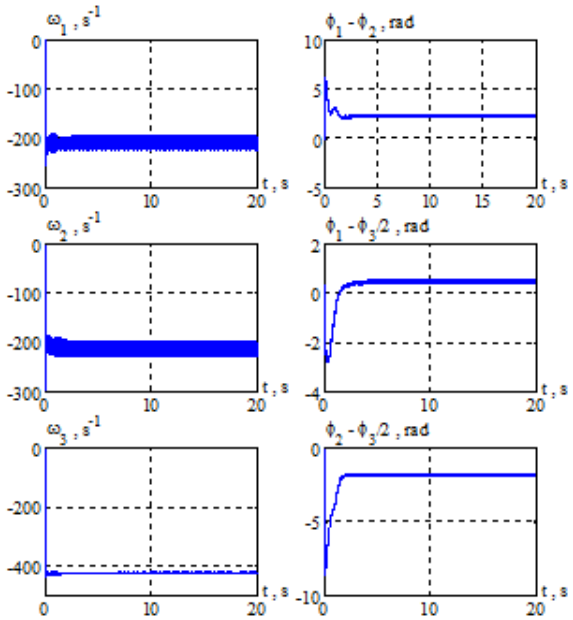

Figure 9. Three-rotor model simulation results for algorithm (7) with $n_1 = n_2 = 1,\ n_3 = 2$.

As seen in diagrams (Fig. 7; Fig. 8), algorithm (7) provides us with stable synchronous rotating mode of rotors at speeds of $\dot{\varphi}_i = 60s^{-1}$, yet algorithm (9) cannot stabilize speeds at needed levels, and some time later they move closer to resonance area $\omega_{res} = 30s^{-1}$.

Fig. 11 and Fig. 12 show motion trajectories of a center of mass of a carrier body with different H^* and n_i.

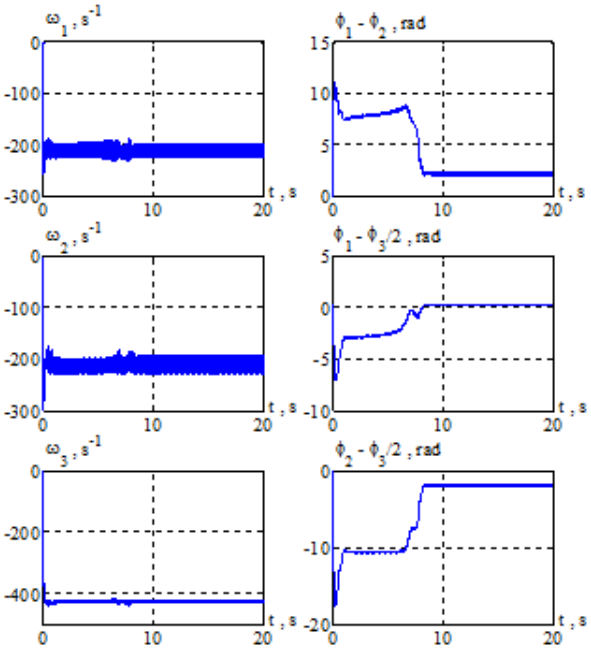

Figure 10. Three-rotor model simulation results for algorithm (9) with $n_1 = n_2 = 1,\ n_3 = 2$.

Simulation results for proposed multiple synchronization control algorithms (7) and (9) in case when speed of a middle rotor is two times higher than speeds of adjacent rotors ($n_1 = n_2 = 1,\ n_3 = 2$) are shown on Fig. 9 and Fig. 10 correspondingly. Research was run at such rotor speed range that it would be far from resonance (given energy value is H^* = 1800 J). As seen in diagrams, the transient time for multiple phase shift ($\varphi_i/n_j - \varphi_j/n_i$), with algorithm (9) is slightly larger. However such a difference in terms of exploitation efficiency for vibration unit control is insignificant.

As seen in formula (1) the steady state behavior of the proposed algorithms is determined by parameters H^* and n_i. The choice of those parameters, at the same time, is determined by technological process requirements, particularly by: requirements for frequency and amplitude of the carrier body oscillations at O_x and O_y axes; shape of the carrier body trajectory, etc. Thus, trajectory of different points on a carrier body during vibrotransportation mode has a shape of ellipse, while during screening of loose materials the amplitude of oscillations along O_x axis strives to zero. The multiple synchronization mode of rotors provides with asymmetric movement of the carrier body that allows us to avoid jamming at the exit of a vibrotransporter if appropriate values of n_i multiplicities are chosen.

Nomograms for dependence of steady-state oscillation amplitudes x_c y_c on nominal energy H^* for various velocity multiplicities are presented in Fig. 13, 14.

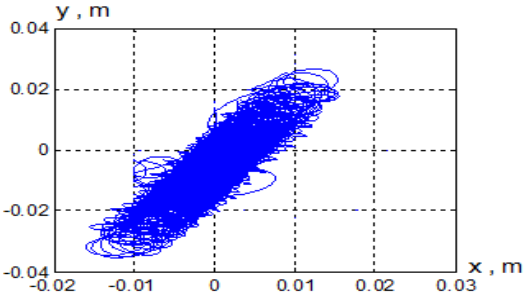

Figure 11. Trajectory of a center of mass of a carrier body with $n_i = 1,\ i = 1,2,3, H^* = 1000J$.

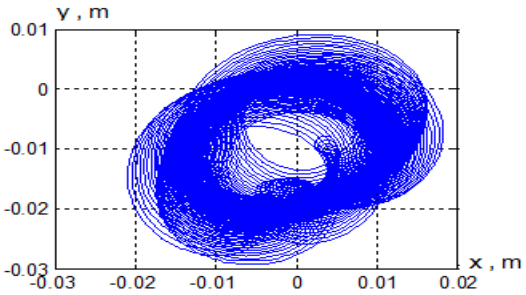

Figure 12. Trajectory of a center of mass of a carrier body with $n_1 = 1, n_2 = 1, n_3 = 2, H^* = 210J$.

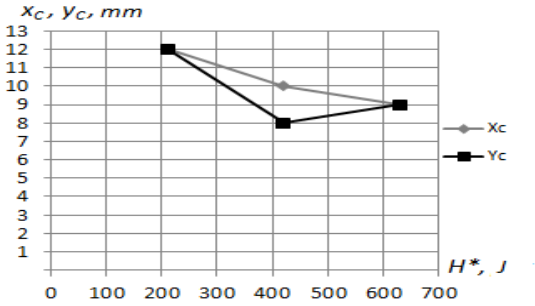

Figure 13. Nomogram of relation between oscillation amplitude of a carrier body at O_x and O_y axes; and given energy H^* for $n_1 = 1, n_2 = 1, n_3 = 2$.

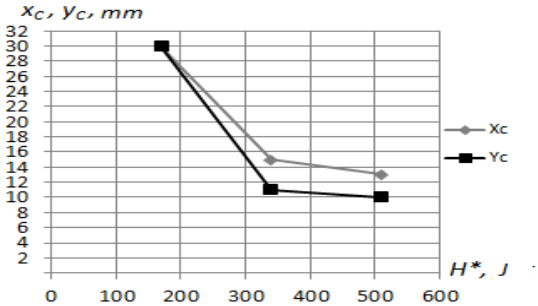

Figure 14. Nomogram of relation between oscillation amplitude of a carrier body at O_x and O_y axes; and given energy H^* for $n_1 = 1, n_2 = 1, n_3 = 3$.

3 Conclusion

The main contribution of our study is design and comparison of two control algorithms providing stable multiple synchronous mode in multi-rotor vibration units with different multiplicities. It is confirmed by numerous simulation results, some of them are presented in the paper. Note that some design and simulation re-

sults for the first algorithm were presented in [Galitskaya and Tomchina, 2012].

Acknowledgments

The work was supported by Russian Foundation for Basic Research (grant 11-08-01218) and Research Program N 1 of OEMMPU Division of RAS.

References

Barkley, D. (1991) A model for fast computer simulation of waves in excitable media. *Physica D*, **49**, pp. 61–70.

Andrievsky, B.R., Blekhman, I.I., Bortsov, Yu.A., Fradkov, A.L., Gavrilov, S.V., Konoplev, V.A., Lavrov, B.P., Polyakhov, N.D., Shestakov, V.M., and Tomchina, O.P. (2001) *Control of Mechatronic Vibration Units* / Eds. Blekhman I.I., Fradkov A.L.. Nauka, St.Petersburg, (in Russian).

Blekhman, I.I. (2000) *Vibrational Mechanics*. Singapore: World Scientific, 510 p.

Blekhman, I.I. (2012) Oscillatory strobodynamics— a new area in nonlinear oscillations theory, nonlinear dynamics and cybernetical physics. *Cybernetics and Physics*, **1**(1), pp. 5–10.

Blekhman, I.I., Fradkov, A.L., Tomchina, O.P., and Bogdanov, D.E. (2002) Self-Synchronization and Controlled Synchronization: General Definition and Example Design. *Mathematics and Computers in Simulation*, **58**(4-6), pp. 367–384.

Czolczynski, K., Perlikowski, P., Stefanski, A., *et al.* (2012) Synchronization of slowly rotating pendulums. *International Journal of Bifurcation and Chaos*, **22**(5), 1250128.

Fradkov, A.L., Andrievsky, B., and Boykov, K.B. (2012) Multipendulum mechatronic setup: Design and experiments. *Mechatronics*, **22**, pp. 76–82.

Fradkov, A.L. (2007) *Cybernetical Physics: From Control of Chaos to Quantum Control*. Springer-Verlag.

Gauthier, J.-P., and Micheau, P. (2008) Extremal harmonic active control of power for rotating machines *Journal of Sound and Vibration*, **318**(4-5), pp. 663–677.

Galitskaya, V.A., and Tomchina, O.P. (2012) Proportional-integral energy-velocity algorithm for multiple synchronization control of vibration unit rotors. *Informatics and Control Systems*, **33**(3), pp. 158–168.

Pena-Ramirez, J., Fey, R., and Nijmeijer, H. (2012) In-phase and anti-phase synchronization of oscillators with Huygens' coupling. *Cybernetics and Physics*, **1**(1), pp. 58–66.

Pogromsky, A.Yu, Belykh, V.N., and Nijmeijer, H. (2003) Controlled synchronization of pendula. *Proc. 42nd IEEE Conference on Decision and Control*, pp. 4381–4386.

Tomchina, O.P, Galitskaya, V.A., and Fradkov, A.L. (2011) Algorithm of multiple synchronization for multi-rotor vibration unit. *7th European Nonlinear Dynamics Conference (ENOC 2011)*, Rome.

Tomchina, O.P., and Kudryavtseva, I.M. (2005) Controlled synchronization of unbalanced rotors with flexible shafts in time-varying vibrational units. *Proc. 2nd Int. Conf. Physics and Control*, St. Petersburg, pp. 790–794.

Ulrichs, H., Mann A., and Parlitz U. (2009) Synchronization and chaotic dynamics of coupled mechanical metronomes. *CHAOS*, **19**(4), Art. No.: 043120.

Wang, D, Zhao, C., Yao, H., *et al.* (2012) Vibration Synchronization of a Vibrating System Driven by Two Motors. *Advances in Vibration Engineering*, **11**(1), pp. 59–73.

Wu, Y., Wang, N., Li, L., *et al.* (2012) Anti-phase synchronization of two coupled mechanical metronomes. *CHAOS*, **22**(2), Art. No. 023146.